Supplemental Data File for:

# Insights into Substrate Specificity and Metal Activation of Mammalian Tetrahedral Aspartyl Aminopeptidase

**Yuanyuan Chen, Erik R. Farquhar, Mark R. Chance, Krzysztof Palczewski and Philip D. Kiser**

## Table of Contents

Table S1. Transcript levels of DNPEP, ENPEP and RAS components in the whole eye and retina of C57BL/6 mice. Data obtained from RNA-seq transcriptome database[a]

| Gene name | Protein name | Whole eye[b] | Retina[c] |
|---|---|---|---|
| Dnpep | Aspartyl aminopeptidase | 73 | 37 |
| Enpep | Glutamyl aminopeptidase | 3.2 | 0.6 |
| Rnpep | Arginine aminopeptidase | 41 | 10 |
| Lnpep | Insulin-responsive aminopeptidase (IRAP) /or Angiotensin IV receptor (AT4) /or leucyl/cystinyl aminopeptidase | 6.3 | 7.1 |
| Agt | Angiotensinogen | 3.7 | 6.5 |
| Ren1[d] | Prorenin/renin | 0 | 0 |
| Ace1 | Angiotensin converting enzyme | 9.0 | 3.6 |
| Ace2 | Angiotensin converting enzyme2 | 1.9 | 0.2 |
| Agt1r | Angiotensin II receptor, type 1 | 0.5 | 0.1 |
| Agtr2 | Angiotensin II receptor, type 2 | 0.03 | 0.06 |
| Rpe65 | RPE65 | 56 | 9.2 |
| Guca1a | Guanylate cyclase activator 1a | 570 | 830 |
| Arrb2 | Arrestin, beta 2 | 8.9 | 11 |
| Rho | Rhodopsin | 6200 | 12000 |

[a] RNA-seq data are taken from NCBI gene expression omnibus site with the series accession number GSE29752. (http://www.ncbi.nlm.nih.gov/projects/geo/query/acc.cgi?accGSE29752). Methods for preparing cDNA library, genome analyzer RNA-seq runs, read mapping, and quantification can be found in (1).

[b] Transcript reads as FPKM (fragments per kilobase normalized by total reads in million) from a cDNA library in the whole eyes of five C57BL/6 female mice at four weeks of age.

[c] Transcript reads as FPKM from a cDNA library prepared from neural retinas of five C57BL/6 female mice at four weeks of age.

[d] The read from Ren1 was zero according to this RNA-seq experiment, which may be due to the low abundance and instability of Ren1 mRNA. However, expression of Ren1 has been reported in the eyes of human, mouse and rat by RT-PCR.

Table S2. Purification of recombinant bovine DNPEP from 1 L of overnight *E. coli* culture

| Step (Unit) | Volume (mL) | Activity (units/mL) | Protein Conc. (mg/mL) | Total Activity (units) | Specific Activity (units/mg) | Recovery (%) |
|---|---|---|---|---|---|---|
| Supernatant | 60 | 6.1 | 40 | 370 | 0.15 | 100 |
| $Ni^{2+}$ column | 5 | 2.3 | 1 | 12[a] | 2.3 | 3.2 |
| Superdex 200 | 20 | 2.5 | 0.33 | 51 | 7.7 | 14 |

[a] Total activity and recovery after elution from $Ni^{2+}$ column is low due to the inhibitory effect of imidazole.

Table S3. Steady-state kinetics of recombinant DNPEP and its Mn-activated form towards Asp-pNA

| | Unit | DNPEP[a] | Mn-act DNPEP[b] |
|---|---|---|---|
| $k_{cat}$ | ($s^{-1}$) | 0.06 | 0.79 |
| $K_M$ | (μM) | 190 | 83 |
| $k_{cat}/K_M$ | ($M^{-1}s^{-1}$) | 300 | 9500 |

[a] Recombinant bovine DNPEP purified from *E.coli* grown in regular LB medium.

[b] Recombinant bovine DNPEP purified from *E.coli* grown in LB medium supplemented with 5 mM $MnCl_2$.

Table S4. Transcript levels of CCK-8 precursor, NKB, MCH precursor and their corresponding receptors in the whole eye and retina of C57BL/6 mice. Data obtained from RNA-seq transcriptome database[a]

| Gene | Protein | Whole eye[b] | Retina[c] |
|---|---|---|---|
| Cck | cholecystokinin | 35 | 20 |
| Cckbr | cholecystokinin B receptor | 1.8 | 4.7 |
| Cckar | cholecystokinin A receptor | 0.22 | 0.13 |
| Tac2 | tachykinin 2 (neurokinin B) | 20 | 30 |
| Tacr3 | tachykinin receptor 3 | 4.1 | 6.3 |
| Pmch | pro-melanin-concentrating hormone | 0.13 | 0 |
| Mchr | melanin-concentrating hormone receptor 1 | 1.8 | 0 |

[a] RNA-seq data are taken from National Center for Biotechnology Information gene expression omnibus site with the series accession number GSE29752. (http://www.ncbi.nlm.nih.gov/projects/geo/query/acc.cgi?accGSE29752). Methods for preparing cDNA library, genome analyzer RNA-seq runs, read mapping, and quantification can be found in reference (1).

[b] Transcript reads as FPKM (fragments per kilobase normalized by total reads in million) from a cDNA library in the whole eyes of five C57BL/6 female mice at four weeks of age.

[c] Transcript reads as FPKM from a cDNA library prepared from neural retinas of five C57BL/6 female mice at four weeks of age.

Table S5. First shell EXAFS analyses of recombinant DNPEP and its Mn-activated form[a]

| ZnZn-DNPEP | | | | | | | | | | | | |
|---|---|---|---|---|---|---|---|---|---|---|---|---|
| | Zn-O/N | | | Zn-N/O | | | Zn•••C | | | | | |
| fit | n | r | $\sigma^2$ | n | r | $\sigma^2$ | n | r | $\sigma^2$ | F'[b] | $\Delta E_0$ | BVS[c] |
| 1 | 3 | 2.01 | 4.0 | | | | | | | 235.1 | -1.96 | 1.30 |
| 2 | 4 | 2.01 | 5.7 | | | | | | | 53.7 | -2.53 | 1.74 |
| **3** | **5** | **2.01** | **7.4** | | | | | | | **27.5** | **-3.21** | **2.19** |
| 4 | 6 | 2.01 | 9.0 | | | | | | | 55.0 | -3.99 | 2.65 |
| 5 | 4 | 1.99 | 4.2 | 1 | 2.13 | -1.0 | | | | 16.1 | -3.83 | 2.25 |
| 6 | 3 | 1.97 | 2.2 | 2 | 2.11 | 0.1 | | | | 15.4 | -2.96 | 2.27 |
| 7 | 5 | 2.00 | 7.4 | | | | 1 | 2.54 | 7.8 | 16.0 | -4.38 | 2.22 |
| 8 | 5 | 2.00 | 7.3 | | | | 0.5 | 2.50 | 2.9 | 22.9 | -4.38 | 2.22 |
| **Mn-activated DNPEP (Zn K-edge)** | | | | | | | | | | | | |
| | Zn-O/N | | | Zn-N/O | | | Zn•••C | | | | | |
| fit | n | r | $\sigma^2$ | n | r | $\sigma^2$ | n | r | $\sigma^2$ | F'[b] | $\Delta E_0$ | BVS[c] |
| 1 | 3 | 1.98 | 2.5 | | | | | | | 146.1 | -5.61 | 1.44 |
| 2 | 4 | 1.98 | 4.1 | | | | | | | 57.1 | -6.10 | 1.92 |
| 3 | 5 | 1.97 | 5.6 | | | | | | | 101.1 | -6.67 | 2.41 |
| 4 | 6 | 1.97 | 7.2 | | | | | | | 288.7 | -7.22 | 2.91 |
| 5 | 3 | 1.97 | 1.2 | 1 | 2.11 | -0.7 | | | | 54.9 | -3.91 | 1.87 |
| 6 | 3 | 1.97 | 2.0 | 2 | 2.11 | 4.7 | | | | 52.0 | -2.74 | 2.28 |
| 7 | 4 | 1.98 | 3.3 | 1 | 2.15 | 2.4 | | | | 48.8 | -3.99 | 2.27 |
| **8** | **4** | **1.97** | **4.2** | | | | **1** | **2.56** | **2.5** | **22.6** | **-6.88** | **1.94** |
| **Mn-activated DNPEP (Mn K-edge)** | | | | | | | | | | | | |
| | Mn-O/N | | | Mn-N/O | | | Mn•••C | | | | | |
| fit | n | r | $\sigma^2$ | n | r | $\sigma^2$ | n | r | $\sigma^2$ | F'[b] | $\Delta E_0$ | BVS[c] |
| 1 | 3 | 2.13 | 4.4 | | | | | | | 37.9 | -0.03 | 1.11 |
| 2 | 4 | 2.13 | 6.6 | | | | | | | 19.5 | -0.78 | 1.49 |
| 3 | 5 | 2.13 | 8.7 | | | | | | | 45.7 | -1.46 | 1.88 |
| 4 | 6 | 2.12 | 10.9 | | | | | | | 133.2 | -2.24 | 2.29 |
| 5 | 4 | 2.12 | 6.3 | 1 | 1.92 | 29.3 | | | | 26.8 | -2.64 | 2.17 |
| 6 | 3 | 2.13 | 4.7 | 2 | 2.04 | 21.7 | | | | 36.1 | -3.47 | 2.08 |
| **7** | **5** | **2.13** | **9.0** | | | | **1** | **2.57** | **2.3** | **16.6** | **-1.66** | **1.87** |
| 8 | 4 | 2.13 | 6.7 | | | | 1 | 2.59 | 1.0 | 7.2 | -1.43 | 1.50 |
| 9 | 4 | 2.14 | 5.1 | 1 | 2.34 | 4.0 | 1 | 2.60 | -1.8 | 5.4 | 1.40 | 1.73 |

[a] r is in units of Å; $\sigma^2$ is in units of $10^{-3}$ Å$^2$; $\Delta E_0$ is in units of eV. All fits are to Fourier-filtered EXAFS data, as follows: ZnZn-DNPEP, Fourier transform range of $k$ = 1.5 – 12.5 Å$^{-1}$, back-transformation range of 0.6 – 2.5 Å (resolution = 0.143 Å); Mn-activated DNPEP (Zn K-edge), Fourier transform range of $k$ = 1.5 – 13.0 Å$^{-1}$, back-transformation range of 0.6 – 2.3 Å.

(resolution = 0.137 Å); Mn-activated DNPEP (Mn K-edge), Fourier transform range of $k$ = 1.5 – 11.25 $Å^{-1}$, back-transformation range of 0.6 – 2.4 Å (resolution = 0.161 Å).

[b] Goodness-of-fit parameter F' defined as $[\Sigma(\chi_{exptl}-\chi_{calc})^2]^2$ / v, where v = $N_{IDP}$ – $N_{VAR}$. $N_{IDP}$ is the number of independent data points, while $N_{VAR}$ is the number of floated variables in each optimization step. F' is a measure of whether an added shell significantly improves the fit.

[c] BVS = bond valence sum for the first-shell atoms of the fit. The BVS is defined as $\Sigma(\exp[(r_0 - r)/0.37])$, where $r_0$ is an empirically derived parameter for a given pair of atoms and r is the actual bond length. The values of $r_0$ were taken from (2) and (3). While EXAFS cannot distinguish between atoms differing by $Z \pm 1$, we assumed an oxygen-rich environment based upon the crystal structure data.

Table S6. Detailed unfiltered EXAFS analysis of recombinant DNPEP at the Zn K-edge[a]

| | Zn-O/N | | | Zn•••C/N/O | | | Zn•••C/Zn | | | Zn•••(His) | | | | | |
|---|---|---|---|---|---|---|---|---|---|---|---|---|---|---|---|
| **fit** | **n** | **r** | **$\sigma^2$** | **n** | **r** | **$\sigma^2$** | **n** | **r** | **$\sigma^2$** | **n** | **r** | **$\sigma^2$** | **F'[b]** | **$\Delta E_0$** | **BVS[c]** |
| 1 | 3 | 2.01 | 4.0 | | | | | | | | | | 0.434 | -1.98 | 1.30 |
| 2 | 4 | 2.01 | 5.7 | | | | | | | | | | 0.371 | -2.37 | 1.74 |
| *3* | *5* | *2.01* | *7.3* | | | | | | | | | | *0.353* | *-3.03* | *2.18* |
| 4 | 6 | 2.01 | 8.9 | | | | | | | | | | 0.368 | -3.62 | 2.64 |
| 5 | 5 | 2.01 | 7.4 | 1 | 2.52 | 7.53 | | | | | | | 0.339 | -3.79 | 2.20 |
| 6 | 5 | 2.01 | 7.2 | | | | 2 | 3.02 | 1.4 | | | | 0.337 | -3.90 | 2.21 |
| 7 | 5 | 2.01 | 7.2 | | | | 3 | 3.03 | 6.0 | | | | 0.348 | -3.92 | 2.21 |
| 8 | 5 | 2.01 | 7.2 | | | | 4<br>4 | 3.05<br>3.28 | 5.6<br>4.1 | | | | 0.307 | -3.38 | 2.19 |
| 9 | 5 | 2.01 | 7.2 | | | | 2<br>4 | 3.00<br>3.18 | 2.1 | | | | 0.320 | -3.14 | 2.20 |
| 10 | 5 | 2.01 | 7.3 | | | | 1Zn | 3.34 | 22.9 | | | | 0.351 | -3.77 | 2.20 |
| **11** | **5** | **2.01** | **7.2** | | | | | | | **1His** | **3.00<br>3.18<br>4.30<br>4.33** | **2.1<br>2.1<br>0.7<br>0.7** | **0.279** | **-3.14** | **2.19** |
| 12 | 5 | 2.01 | 7.3 | | | | | | | 2His | 3.00<br>3.18<br>4.29<br>4.32 | 6.7<br>6.7<br>6.3<br>6.3 | 0.295 | -3.13 | 2.19 |
| 13 | 5 | 2.01 | 7.2 | | | | 1Zn | 3.20 | 15.2 | 1His | 3.01<br>3.19<br>4.30<br>4.33 | 1.5<br>1.5<br>0.8<br>0.8 | 0.271 | -3.20 | 2.19 |

[a] r is in units of Å; $\sigma^2$ is in units of $10^{-3}$ Å$^2$; $\Delta E_0$ is in units of eV. All fits are to unfiltered EXAFS data for a Fourier transform range of $k$ = 1.5 – 12.5 Å$^{-1}$ (resolution = 0.144 Å).

[b] $F = [\Sigma k^6(\chi_{exptl}-\chi_{calc})^2 / \Sigma k^6 \chi_{exptl}^2]^{1/2}$

[c] BVS = bond valence sum for the first-shell atoms of the fit. The BVS is defined as $\Sigma(\exp[(r_0 - r)/0.37])$, where $r_0$ is an empirically derived parameter for a given pair of atoms and r is the actual bond length. The values of $r_0$ were taken from (2) and (3). While EXAFS cannot distinguish between atoms differing by $Z \pm 1$, we assumed an oxygen-rich environment based upon the crystal structure data.

Table S7. Fourier-filtered EXAFS analyses of Mn-activated DNPEP at the Zn K-edge[a]

| | Zn-O/N | | | Zn•••C/N/O | | | Zn•••C | | | Zn•••Mn | | | | | |
|---|---|---|---|---|---|---|---|---|---|---|---|---|---|---|---|
| **fit** | **n** | **r** | **$\sigma^2$** | **n** | **r** | **$\sigma^2$** | **n** | **r** | **$\sigma^2$** | **n** | **r** | **$\sigma^2$** | **F' [b]** | **$\Delta E_0$** | **BVS[c]** |
| 1 | 3 | 1.97 | 2.4 | | | | | | | | | | 288.1 | -5.95 | 1.44 |
| 2 | 4 | 1.97 | 4.0 | | | | | | | | | | 186.1 | -6.13 | 1.92 |
| 3 | 5 | 1.97 | 5.6 | | | | | | | | | | 250.3 | -6.66 | 2.41 |
| 4 | 6 | 1.97 | 7.1 | | | | | | | | | | 460.7 | -7.20 | 2.91 |
| 5 | 4 | 1.98 | 3.1 | 1N | 2.17 | 1.4 | | | | | | | 172.3 | -3.32 | 2.23 |
| 6 | 3 | 1.97 | 1.2 | 1N | 2.12 | -0.3 | | | | | | | 186.9 | -3.83 | 1.86 |
| *7* | *4* | *1.97* | *4.1* | *1C* | *2.53* | *2.0* | | | | | | | *145.1* | *-7.02* | *1.94* |
| 8 | 4 | 1.97 | 4.0 | | | | | | | 1Mn | 3.31 | 5.5 | 77.6 | -6.58 | 1.93 |
| 9 | 4 | 1.98 | 3.2 | 1 | 2.16 | 2.0 | | | | 1Mn | 3.32 | 5.4 | 64.8 | -4.31 | 2.27 |
| *10* | *4* | *1.97* | *4.1* | *1C* | *2.54* | *3.0* | | | | *1Mn* | *3.30* | *5.5* | *46.7* | *-7.27* | *1.95* |
| 11 | 4 | 1.97 | 4.2 | 1C | 2.55 | 2.1 | 2 | 3.01 | 0.8 | | | | 104.5 | -6.58 | 1.93 |
| 12 | 4 | 1.97 | 4.1 | 1C | 2.54 | 2.4 | 4 | 3.00 | 5.6 | | | | 179.4 | -6.91 | 1.94 |
| 13 | 4 | 1.97 | 4.1 | 1C | 2.54 | 3.8 | 2 | 3.31 | 0.0 | | | | 65.0 | -7.32 | 1.95 |
| 14 | 4 | 1.97 | 4.1 | 1C | 2.54 | 3.4 | 4 | 3.31 | 3.1 | | | | 69.4 | -7.37 | 1.95 |
| 15 | 4 | 1.97 | 4.1 | 1C | 2.55 | 3.9 | 4<br>4 | 3.03<br>3.30 | 7.7<br>3.2 | | | | 44.1 | -7.03 | 1.94 |
| 16 | 4 | 1.97 | 4.1 | 1C | 2.54 | 3.1 | 2 | 3.02 | 2.7 | 1Mn | 3.29 | 7.0 | 33.4 | -7.16 | 1.94 |
| **17** | **4** | **1.97** | **4.1** | **1C** | **2.54** | **3.3** | **4** | **3.07** | **12.0** | **1Mn** | **3.29** | **4.8** | **41.3** | **-7.53** | **1.94** |

[a] r is in units of Å; $\sigma^2$ is in units of $10^{-3}$ Å$^2$; $\Delta E_0$ is in units of eV. All fits are to Fourier-filtered EXAFS data for a Fourier transform range of $k$ = 1.5 – 13.0 Å$^{-1}$ and back-transformation range of 0.6 – 3.1 Å (resolution = 0.137 Å).

[b] Goodness-of-fit parameter F' defined as $[\Sigma(\chi_{exptl}-\chi_{calc})^2]^2 / v$, where $v = N_{IDP} - N_{VAR}$. $N_{IDP}$ is the number of independent data points, while $N_{VAR}$ is the number of floated variables in each optimization step. F' is a measure of whether an added shell significantly improves the fit.

[c] BVS = bond valence sum for the first-shell atoms of the fit. The BVS is defined as $\Sigma(\exp[(r_0 - r)/0.37])$, where $r_0$ is an empirically derived parameter for a given pair of atoms and r is the actual bond length. The values of $r_0$ were taken from (2) and (3). While EXAFS cannot distinguish between atoms differing by $Z \pm 1$, we assumed an oxygen-rich environment based upon the crystal structure data.

Table S8. Fourier-filtered EXAFS analyses of Mn-activated DNPEP at the Mn K-edge[a]

| | Mn-O/N | | | Mn•••C/N/O | | | Mn•••C | | | Mn•••Zn | | | | | |
|---|---|---|---|---|---|---|---|---|---|---|---|---|---|---|---|
| **fit** | **n** | **r** | **$\sigma^2$** | **n** | **r** | **$\sigma^2$** | **n** | **r** | **$\sigma^2$** | **n** | **r** | **$\sigma^2$** | **F'** [b] | **$\Delta E_0$** | **BVS**[c] |
| 1 | 3 | 2.14 | 4.4 | | | | | | | | | | 59.9 | 0.17 | 1.10 |
| 2 | 4 | 2.13 | 6.6 | | | | | | | | | | 41.5 | -0.52 | 1.48 |
| 3 | 5 | 2.13 | 8.7 | | | | | | | | | | 68.2 | -1.20 | 1.87 |
| 4 | 6 | 2.12 | 10.9 | | | | | | | | | | 142.5 | -1.93 | 2.27 |
| **5** | **5** | **2.13** | **9.0** | **1** | **2.56** | **2.10** | | | | | | | **38.9** | **-1.18** | **1.86** |
| 6 | 4 | 2.13 | 6.7 | 1 | 2.58 | 1.40 | | | | | | | 29.6 | -0.92 | 1.49 |
| 7 | 5 | 2.13 | 8.7 | | | | | | | 1Zn | 3.40 | 10.6 | 54.2 | -1.60 | 1.88 |
| *8* | *5* | *2.13* | *9.0* | *1* | *2.56* | *2.80* | | | | *1Zn* | *3.41* | *12.0* | *29.5* | *-1.07* | *1.85* |
| 8a | 5 | 2.13 | 8.9 | 1 | 2.56 | 2.97 | | | | 0.5Zn | 3.41 | 7.3 | 31.1 | -1.17 | 1.86 |
| 9 | 5 | 2.14 | 9.0 | 1 | 2.56 | 3.34 | 2 | 3.43 | 4.9 | | | | 51.8 | -0.25 | 1.83 |
| 10 | 5 | 2.13 | 9.0 | 1 | 2.56 | 2.31 | 2 | 3.07 | 9.3 | | | | 32.3 | -0.62 | 1.84 |
| 11 | 5 | 2.14 | 9.0 | 1 | 2.56 | 2.66 | 4 | 3.11 | 24.3 | | | | 32.9 | -0.27 | 1.83 |
| 12 | 5 | 2.14 | 9.1 | 1 | 2.55 | 3.09 | 2<br>2 | 3.10<br>3.40 | 7.8<br>8.0 | | | | 33.2 | 0.56 | 1.81 |
| *13* | *5* | *2.14* | *9.0* | *1* | *2.56* | *3.19* | *2* | *3.12* | *12.0* | *1Zn* | *3.40* | *12.2* | *22.1* | *-0.28* | *1.83* |
| 14 | 5 | 2.14 | 8.9 | 1 | 2.56 | 3.37 | 2 | 3.11 | 14.1 | 0.5Zn | 3.40 | 7.8 | 25.4 | -0.38 | 1.83 |
| 15 | 5 | 2.14 | 9.0 | 1 | 2.56 | 3.55 | 4 | 3.14 | 20.6 | 1Zn | 3.41 | 11.4 | 19.2 | 0.03 | 1.82 |

[a] r is in units of Å; $\sigma^2$ is in units of $10^{-3}$ Å$^2$; $\Delta E_0$ is in units of eV. All fits are to Fourier-filtered EXAFS data for a Fourier transform range of $k$ = 1.5 – 11.25 Å$^{-1}$ and back-transformation range of 0.6 – 3.4 Å (resolution = 0.164 Å).

[b] Goodness-of-fit parameter F' defined as $[\Sigma(\chi_{exptl}-\chi_{calc})^2]^2 / v$, where $v = N_{IDP} - N_{VAR}$. $N_{IDP}$ is the number of independent data points, while $N_{VAR}$ is the number of floated variables in each optimization step. F' is a measure of whether an added shell significantly improves the fit.

[c] BVS = bond valence sum for the first-shell atoms of the fit. The BVS is defined as $\Sigma(\exp[(r_0 - r)/0.37])$, where $r_0$ is an empirically derived parameter for a given pair of atoms and r is the actual bond length. The values of $r_0$ were taken from (2) and (3). While EXAFS cannot distinguish between atoms differing by $Z \pm 1$, we assumed an oxygen-rich environment based upon the crystal structure data.

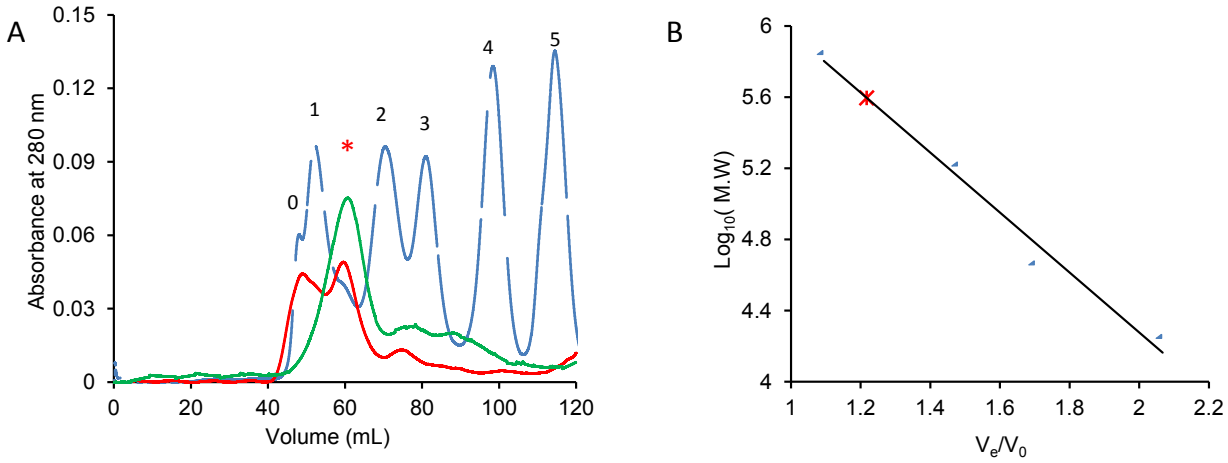


Figure S1. Gel filtration chomatography of DNPEP. A, Gel filtration chromatograms showing the profiles before (red line) and after (green line) optimization of the purification protocol relative to molecular weight standards (blue dashed line, 0, void volume; 1, Thyroglobulin (670 kDa); 2, Bovine gamma-globulin (158 kDa); 3, Chicken ovalbumin (44 kDa); 4 Equine myoglobin (17 kDa); 5, Vitamin $B_{12}$ (1.35 kDa)). B, Linear plot of the logarithm of molecular weight as a function of elution-to-void volume ratio of protein standards. DNPEP eluted at apparent molecular mass of ~394 kDa (red asterisk), which corresponds to a stoichiometry of 7.3±0.9 subunits assuming a monomer mass of 54 kDa. The error was calculated as combined errors of standard deviation and curve fitting.

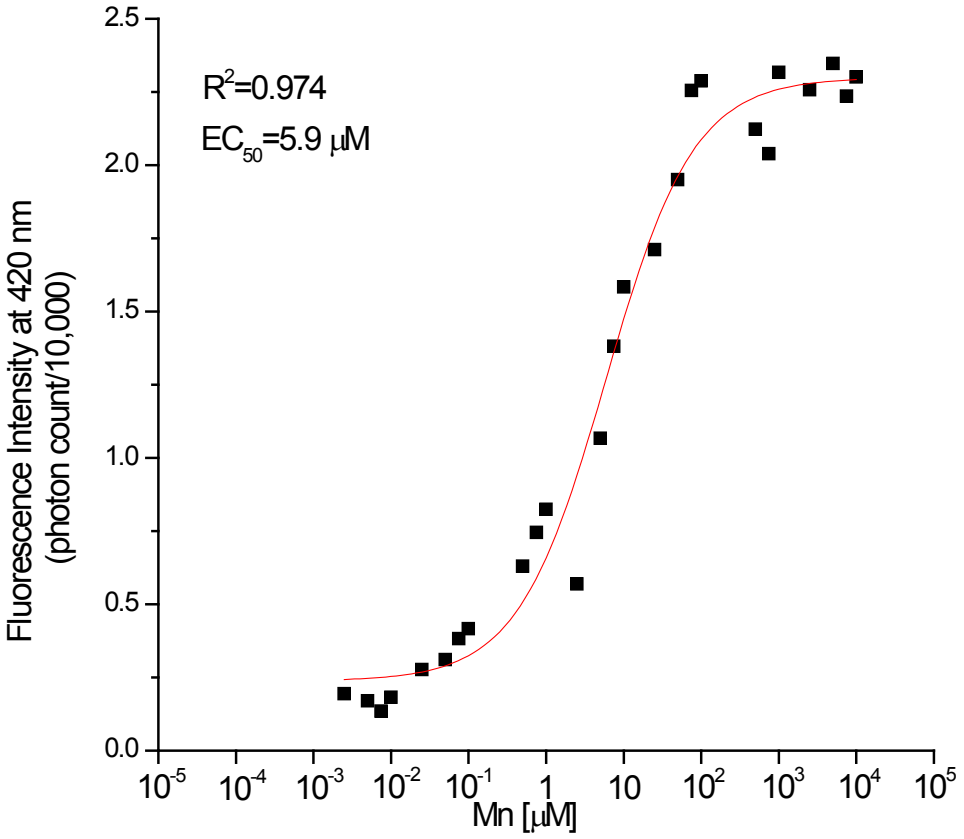


Figure S2. Dose-effect curve of DNPEP activity stimulation by Mn. $MnCl_2$ was added to final concentrations ranging from 2.5 nM to 10 mM and activity of DNPEP was measured as described in the Experimental Procedures. Activity was quantified as the fluorescence intensity at 420 nm at the end of the 30 min reaction. The results are presented on a semi-logarithmic graph. The $EC_{50}$ of Mn was calculated as ~6 μM by pharmacology dose-response fitting in Origin 8.1. $MnCl_2$ concentrations greater than 25 mM inhibit DNPEP activity.

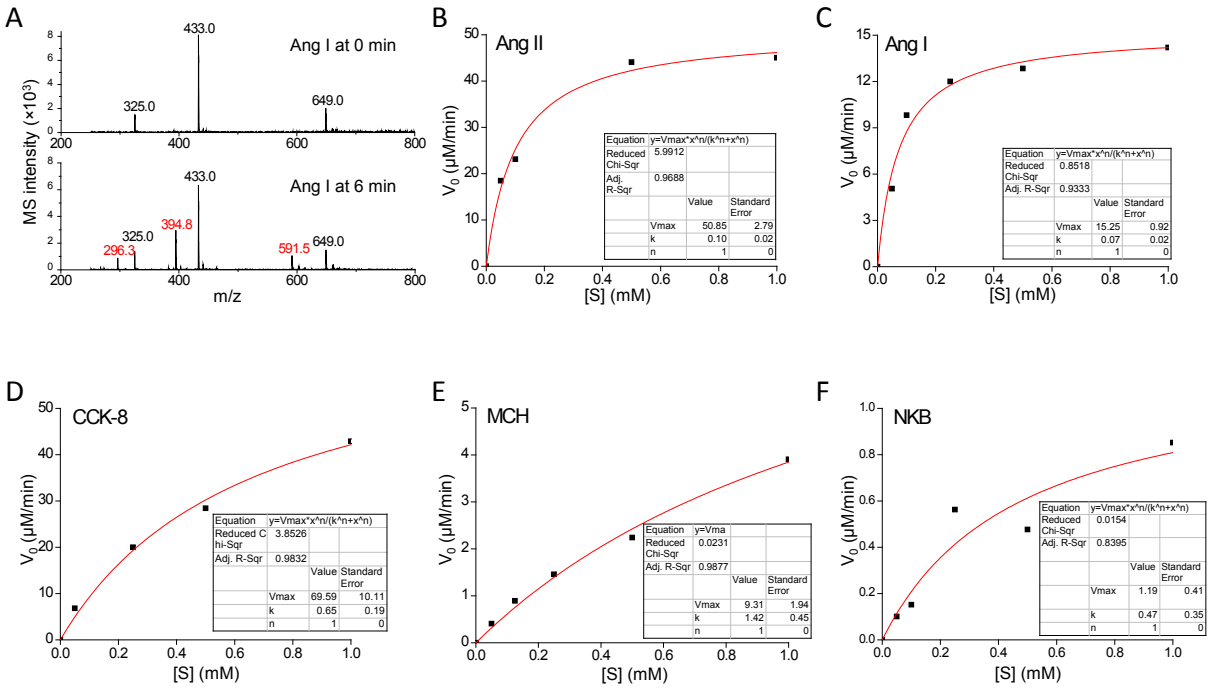


Figure S3. DNPEP catalyzed hydrolysis of physiologically relevant peptides by LC-MS. A. Mass spectra showing 0.5 mM Ang I before and 6 min after addition of DNPEP. Peaks with black labels are due to Ang I with +2, +3, and +4 charges; and peaks with red labels observed after addition of DNPEP are due to product Ang (2-10) with +2, +3, and +4 charges. The Michealis-Menten fits for steady-state hydrolysis of Ang I, Ang II, CCK-8, MCH, and NKB are shown in B to F, respectively. Fits were performed using the Sigmoidal-Hill function in Origin 8.1, and fitting results were listed in the inset tables. Detailed calculations are described in Experimental Procedures.

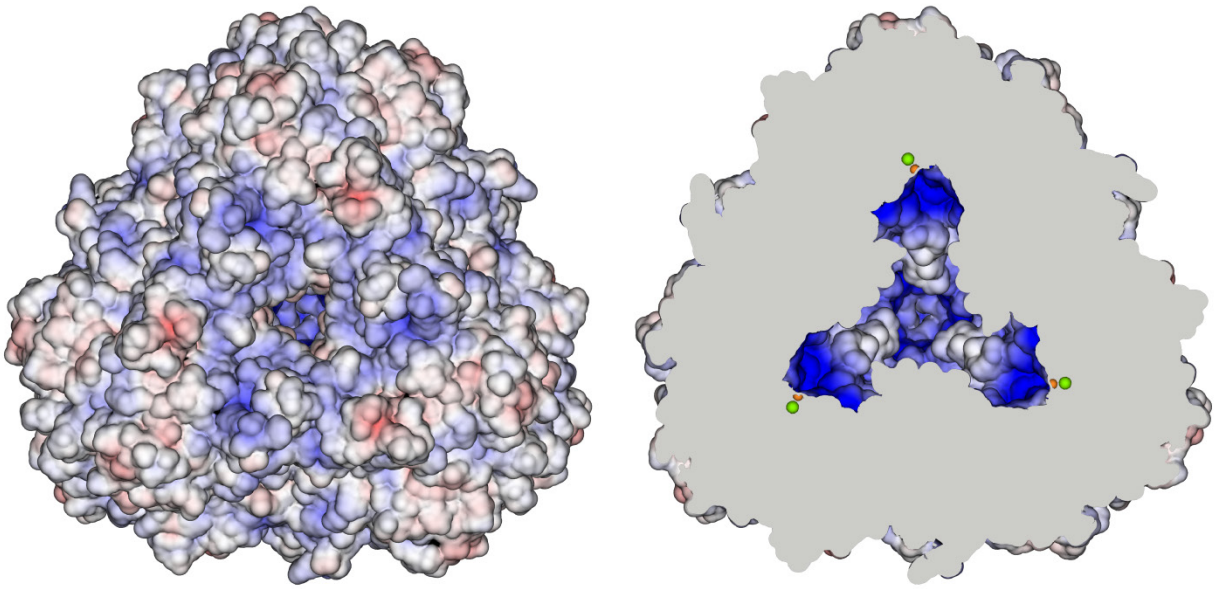

Figure S4. Electrostatic surface potential of the DNPEP complex. A. Exterior surface potential showing the fairly uniform charge distribution on the outside surface of the complex. B. A slice-through view of the tetrahedral complex showing a strongly positive potential, particularly in the vicinity of the active site pocket. The electrostatic potential is contoured at -10 kT/e (red) and 10 kT/e (blue). The positive electrostatic potential of the active site pocket is in agreement with the preference of the enzyme for N-terminal acidic peptide substrates. The electrostatic potential was calculated using APBS (4).

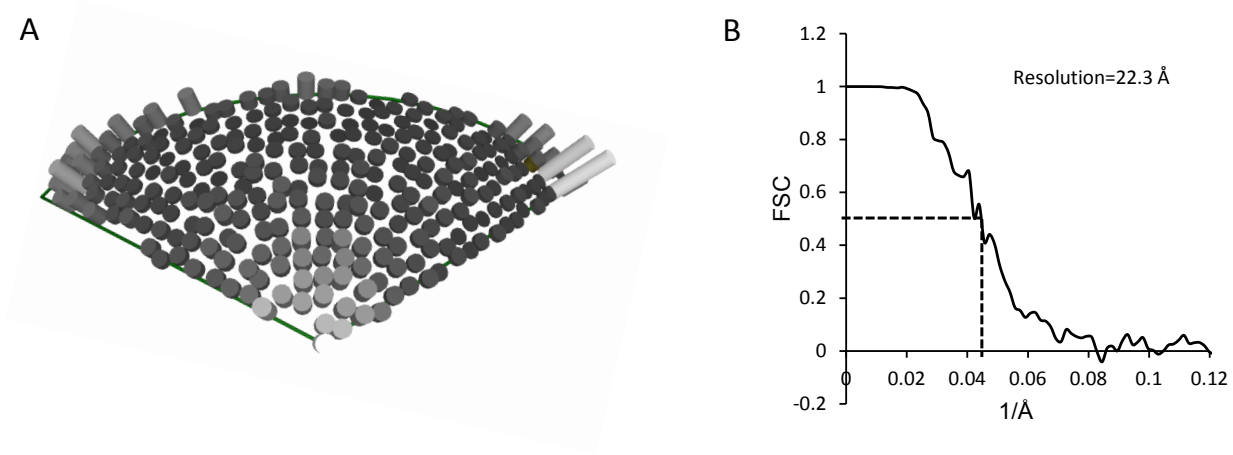


Figure S5. Completeness and resolution of the EM data set used for single particle reconstruction. A, Euler distribution plot of the data set showing a complete angular coverage of the unique projection space. B, Fourier Shell Correlation (FSC) plot obtained from an even/odd test in EMAN2 showing a resolution of 22.3 Å according to the 0.5 criterion.

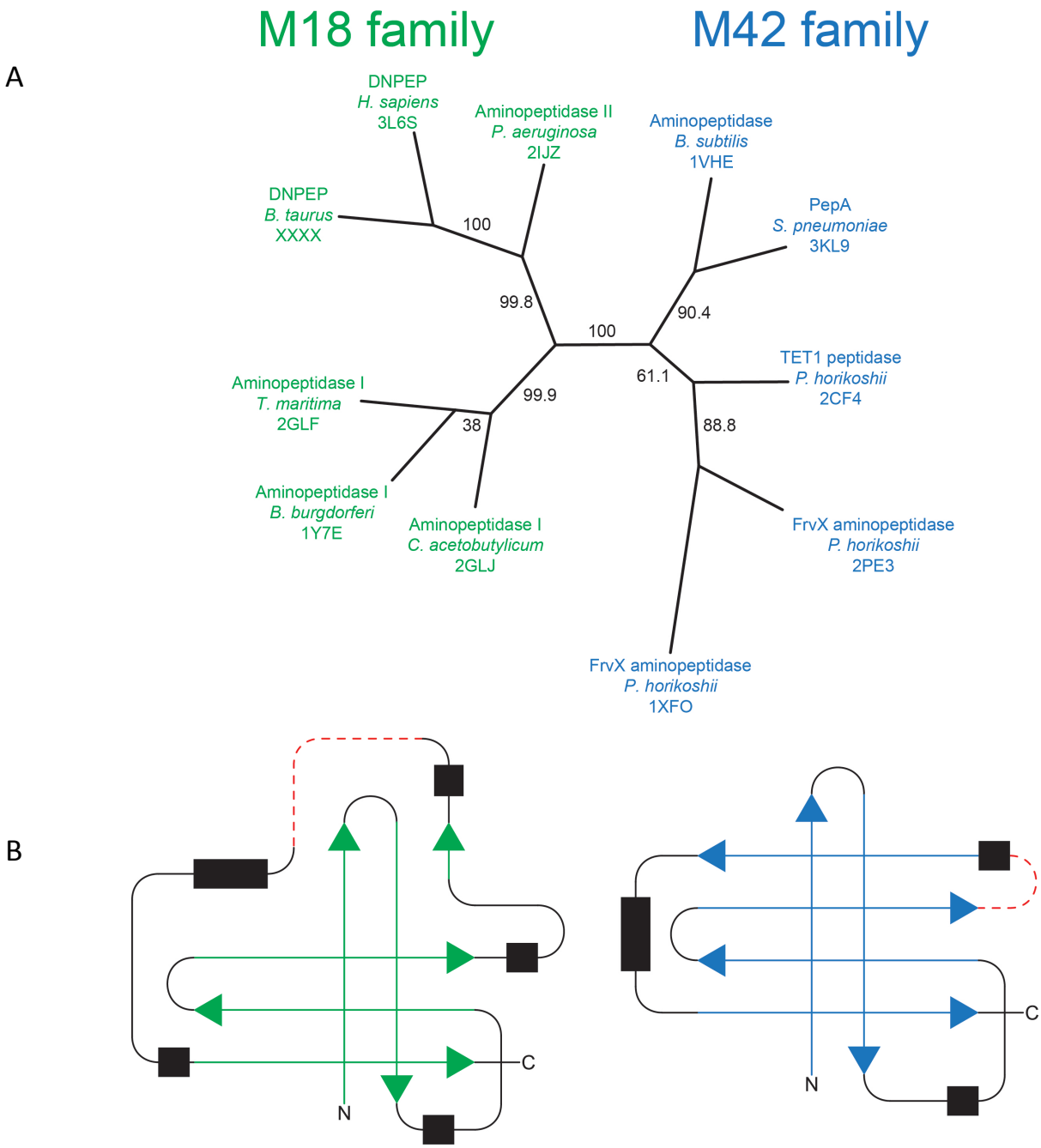


Figure S6. Comparison of the M18 and M42 aminopeptidases. A, An unrooted phylogenetic tree of crystallographically characterized peptidases from the two families. Sequences were aligned using *Clustal omega* (5) and the phylogeny was computed using the *Proml* and *Consense* programs from the PHYLIP package (6). Bootstrap values from 1000 replicates are displayed on the tree branches as percentages. B, topologies of dimerization domains in the two families. M18 family is colored in green, and M42 family is in blue.

Movie S1. Structure of the DNPEP monomer and tetrahedral assembly. This movie shows the overall structure of DNPEP, the close proximity of $His^{166}$ from one monomer to the active site of an adjacent monomer related by two-fold symmetry, the dimeric and trimeric interaction surfaces and finally the tetrahedral assembly.

Supplemental References

1. Mustafi, D., Kevany, B. M., Genoud, C., Okano, K., Cideciyan, A. V., Sumaroka, A., Roman, A. J., Jacobson, S. G., Engel, A., Adams, M. D., and Palczewski, K. (2011) Defective photoreceptor phagocytosis in a mouse model of enhanced S-cone syndrome causes progressive retinal degeneration. *FASEB J.* **25**, 3157-3176
2. Brown, I. D., and Altermatt, D. (1985) Bond-valence parameters obtained from a systematic analysis of the Inorganic Crystal Structure Database. *Acta Crystallogr. B* **41**, 244-247
3. Liu, W., and Thorp, H. H. (1993) Bond valence sum analysis of metal-ligand bond lengths in metalloenzymes and model complexes. 2. Refined distances and other enzymes. *Inorg. Chem.* **32**, 4102-4105
4. Baker, N. A., Sept, D., Joseph, S., Holst, M. J., and McCammon, J. A. (2001) Electrostatics of nanosystems: application to microtubules and the ribosome. *Proc. Natl. Acad. Sci. U. S. A.* **98**, 10037-10041
5. Sievers, F., Wilm, A., Dineen, D., Gibson, T. J., Karplus, K., Li, W. Z., Lopez, R., McWilliam, H., Remmert, M., Soding, J., Thompson, J. D., and Higgins, D. G. (2011) Fast, scalable generation of high-quality protein multiple sequence alignments using Clustal Omega. *Mol. Syst. Biol.* **7**
6. Felsenstein, J. (2005) PHYLIP (Phylogeny Inference Package) version 3.6.